

The Effect of Variation Resistance Broken Bars in Induction Motor Using Stator Current Signature Analysis

A. Menacer ⁽¹⁾, M. S. Nait Said ⁽²⁾, A. H. Benakcha ⁽¹⁾, S. Moreau ⁽³⁾, S. Drid ⁽²⁾

⁽¹⁾ Laboratoire de Génie Electrique de Biskra LGEB, Département d'Electrotechnique de l'Université de Biskra, B.p 145, Biskra, 07000, Algeria

⁽²⁾ Laboratory LSPIE Propulsion-Induction Electromagnetic, Department of Electrical Engineering 05000 Batna University, Algeria.

⁽³⁾ Laboratoire d'Automatique et d'Informatique Industrielle LAII, ESIP, 40 avenue du Recteur Pineau, 86022 Poitiers cedex, France.
e.mail: Menacer_arezki@hotmail.com

Abstract - In all mechanical devices, motors are subject to failures, which can sometimes lead to the shutting down of an entire industrial process. That is the reason why predictive maintenance and prognosis are necessary. Motor current signature analysis is a condition monitoring technique that is now widely used to diagnose problems such as broken rotor bars, abnormal levels of airgap eccentricity, shorted turns in low voltage stator windings and some mechanical problems.

This paper presents the effect of the broken bar time evolution since the created incipient fault on the various characteristics of the induction machine such as torque, speed and currents. The induction motor is simulated while the rotor bar resistance is varying linearly versus time since its normal value to the final broken bar situation (partial to total broken bar).

The methods used for analysis are based on:

- the *Lissajous* representation of *Park* vector current components
- spectral analysis of stator current and the modulus of *Park* vector current

By this way, we can observe the incipient fault impact on the different characteristics of the machines such as torque, speed and currents.

Keywords: Fault simulation, condition monitoring, induction motors, broken bar; resistance bar; incipient fault, *Park* extended vector current, modulus, stator current.

1. Introduction

The problem of diagnosis is related to maintenance, which requires defining economic factors, which are generally difficult to evaluate. The issues of preventive and condition-based maintenance, on line monitoring, system fault detection, diagnosis and prognosis become of increasing importance.

The key conditions for a successful motor operation are a quality motor well suited to its application and with its proper maintenance. The use of induction motors in today's industry is extensive and they can be exposed to different hostile environments, manufacturing defects, etc...

[1].

Rotor faults may occur particularly in high power machines. These defects have two causes: first, high temperatures and large centrifugal forces produced during transient operations such as startup; and secondly, manufacturing flaws such as defective casting and poor end-ring joints.

The problem of broken bars in induction motors stations of offshore oilrig pumping, which were at the origin of the first research tasks on the diagnosis, is a good example [2]. Several works followed in the same way [3-6], or were initiated in the diagnosis of other failures of the machine such as rotor eccentricity [7], open circuits [8], [9], [5], wear of the stages [10], [11].

These types of faults usually refer to the gradual deterioration of the motor, which can lead to motor failure if undetected [1].

Monitoring the current per-phase can provide the indications on the motors state. This is preferable, compared to other methods since it is easy for physics measurements. The fault is highlighted by the spectral current signal when the induction machine is sufficiently loaded and generally, we can extract from it the number of the broken bars [6].

Faults detection based on motor current analysis relies on interpretation of the frequency components in the current spectrum, which are related to rotor asymmetries.

Spectral analyses of stator current [17] [19], or of the *Park* vector current and modulus are also considered in diagnosis [14]. But it requires knowledge of motor electrical parameters, which are affected by different physical phenomena, such as temperature variations, skin effects, core losses and saturation. In diagnosis, we examine different approaches to the spectral analysis of stator current.

Reference [15] examines the spectral analysis of the *Park* vector current modulus, which uses the fact that the spectrum does not contain a fundamental component, but only relative frequencies directly linked to the fault, thus making these components easier to identify.

In order to study phenomena taking place in the rotor, the last one is currently modeled in the form of N_R meshes as shown in Fig. 1.

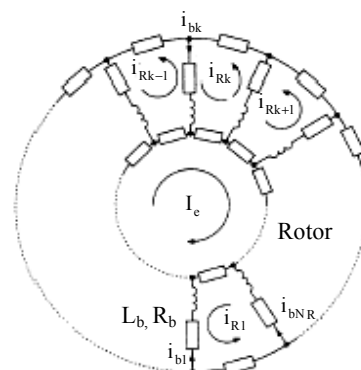


Fig. 1: Rotor cage equivalent circuit

2. Inductances in induction motors

The model assumptions are:

- negligible saturation and skin effect,
- uniform air-gap,
- sinusoidal stator windings mmf in air-gap,
- rotor bars insulation (no inter bar current flows through the laminations),
- infinite relative permeability of machine armatures.

Although a sinusoidal mmf of stator winding is assumed, other winding distributions could also be analyzed by simply using superposition. It is justified by the fact that different space harmonic components do not interact [12].

To study the performance of squirrel cage induction motors with rotor fault, a mesh model of the rotor is selected as illustrated in Fig.1 [12]. This induction machine model takes into account the effective geometry of the rotor. The squirrel cage rotor is described as a system of (N_R+1) identical and evenly spaced loops. The inductances are conveniently computed by means of an analytical approach. Generally, this approach is based on a linear flux current relation.

A. Stator inductances

The phase mmf expression is given in the following relation [13]:

$$F_n(\theta) = \frac{2}{\pi} \cdot \frac{N_S i_{Sn}}{p} \cos(p\theta - (n-1)\frac{2\pi}{3}) \quad (1)$$

By means of the above-mentioned assumptions, the fundamental of the radial flux density in the air-gap can be written as:

$$B_{Sn} = \frac{2\mu_0}{\pi e} \frac{N_S}{p} i_{Sn} \cos(p\theta - (n-1)\frac{2\pi}{3}) \quad (2)$$

The main flux is thus written as:

$$\Phi_{Spn} = \frac{4\mu_0}{\pi e} \frac{N_S^2}{p^2} r_g \cdot l \cdot i_{Sn} \quad (3)$$

The principal magnetizing inductance of each stator phase is:

$$L_{Sp} = \frac{\Phi_{Spn}}{i_{Sn}} = \frac{4\mu_0}{\pi e} \frac{N_S^2}{p^2} r_g \cdot l \quad (4)$$

The total phase inductance is therefore equal to the sum of the magnetizing and leakage inductances such as:

$$L_S = L_{Sp} + L_{Sf} \quad (5)$$

The mutual inductance between stator phases is given by:

$$M_s = \frac{-L_{Sp}}{2} \quad (6)$$

B. Rotor inductances

The form of magnetic induction produced by a rotor mesh in the air-gap is supposed radial and it is represented in Fig. 2.

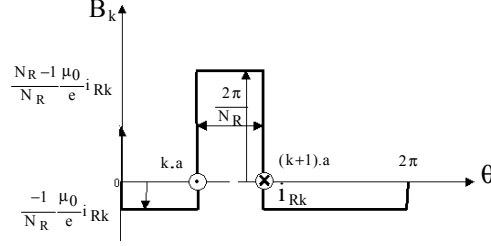


Fig. 2: Form of magnetic induction of rotor mesh created by two bars

The principal inductance of a rotor mesh can be calculated from magnetic induction distribution as done in Fig. 2 [13]:

$$L_{Rp} = \frac{N_R - 1}{N_R^2} \frac{\mu_0}{e} 2\pi r_g l \quad (7)$$

The self and mutual rotor loops are obtained by considering each rotor loop k as an elementary mesh with a loop current.

The total inductance of the k^{th} rotor mesh is equal to the sum of its principal inductance and leakage inductance of the two bars and leakage inductance of the two portions of rings of short circuit closing the mesh k as indicated in Fig. 3.

$$L_{RR} = L_{Rp} + 2L_b + 2L_e \quad (8)$$

The mutual inductance between nonadjacent rotor meshes is given by the following relation deduced from the scheme of Fig. 3

$$M_{RR} = -2\pi \frac{\mu_0}{e} \frac{r_g l}{N_R^2} \quad (9)$$

The k^{th} mutual inductance between the adjacent meshes can be written as:

$$M_{Rk(k-1)} = M_{Rk(k+1)} = M_{RR} - L_b \quad (10)$$

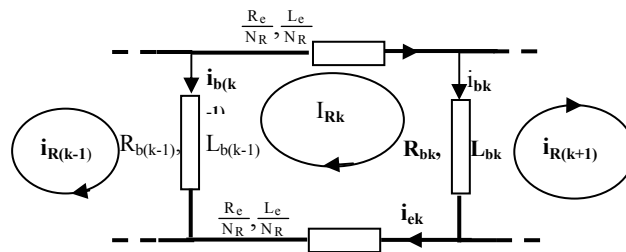


Fig. 3: Electric diagram equivalent of a rotor mesh

In the same manner, the stator rotor mutual between the stator phase "l" and the kth rotor loop can be calculated using the flux linked to the rotor loop and is given by:

$$M_{RkSl_n} = -M_{SR} \cos\left(\theta - (n-1)\frac{2\pi}{3} + ka\right) \quad (11)$$

where:

$$a = \frac{2\pi}{N_R} \cdot p \quad \text{and} \quad M_{SR} = \frac{4\mu_0}{\pi} \frac{N_S I_g l}{e p^2} \sin\left(\frac{a}{2}\right)$$

3. Squirrel cage induction motor modeling mesh

The mathematical model of squirrel cage induction motor can be written as:

$$[V] = [R][I] + \frac{d}{dt}([L][I]) \quad (12)$$

where:

$$[V] = \begin{bmatrix} [V_S] \\ [V_R] \end{bmatrix}, \quad [I] = \begin{bmatrix} [I_S] \\ [I_R] \end{bmatrix}$$

with:

$$\begin{aligned} [V_S] &= [V_{S1} \ V_{S2} \ V_{S3}]^T \\ [V_R] &= [0 \ 0 \ 0 \ \dots \ 0]_{1 \times N_R + 1}^T \\ [I_S] &= [I_{S1} \ I_{S2} \ i_{S3}]^T \\ [I_R] &= [I_{R1} \ I_{R2} \ \dots \ I_{Rk} \ \dots \ I_{RN_R} \ I_e]^T \end{aligned}$$

The global resistance matrix can be written as:

$$[R] = \begin{bmatrix} [R_S]_{3 \times 3} & \vdots & [0]_{3 \times N_R} & \vdots & [0]_{3 \times 1} \\ \dots & \dots & \dots & \dots & \dots \\ [0]_{N_R \times 3} & \vdots & [R_R]_{N_R \times N_R} & \vdots & -\frac{R_e}{N_R} [1]_{N_R \times 1} \\ \dots & \dots & \dots & \dots & \dots \\ [0]_{1 \times 3} & \vdots & -\frac{R_e}{N_R} [1]_{1 \times N_R} & \vdots & R_e \end{bmatrix} \quad (13)$$

where:

$$[R_S]_{3 \times 3} = \begin{bmatrix} R_S & 0 & 0 \\ 0 & R_S & 0 \\ 0 & 0 & R_S \end{bmatrix}$$

and

$$[\mathbf{R}_R]_{N_R \times N_R} = \begin{bmatrix} R_{b0} + R_{b(N_R-1)} + 2\frac{L_c}{N_R} - R_{b0} & 0 & \dots & \dots & \dots & -R_{b(N_R-1)} \\ 0 & \dots & -R_{b(k-1)} & R_{bk} + R_{b(k-1)} + 2\frac{L_c}{N_R} - R_{bk} & 0 & \dots & 0 \\ \dots & \dots & \dots & \dots & \dots & \dots & \dots \\ -R_{b(N_R-1)} & 0 & \dots & \dots & 0 & -R_{b(N_R-2)} & R_{b(N_R-1)} + R_{b(N_R-2)} + 2\frac{L_c}{N_R} \end{bmatrix}$$

The complete matrix inductance can be represented by:

$$[\mathbf{L}] = \begin{bmatrix} [\mathbf{L}_S]_{3 \times 3} & \vdots & [\mathbf{M}_{SR}]_{3 \times N_R} & \vdots & [\mathbf{0}]_{3 \times 1} \\ \dots & \dots & \dots & \dots & \dots \\ [\mathbf{M}_{RS}]_{N_R \times 3} & \vdots & [\mathbf{L}_R]_{N_R \times N_R} & \vdots & -\frac{L_e}{N_R} [\mathbf{1}]_{N_R \times 1} \\ \dots & \dots & \dots & \dots & \dots \\ [\mathbf{0}]_{1 \times 3} & \vdots & -\frac{L_e}{N_R} [\mathbf{1}]_{1 \times N_R} & \vdots & L_e \end{bmatrix} \quad (14)$$

where:

$$[\mathbf{L}_S]_{3 \times 3} = \begin{bmatrix} L_{Sp} & M_S & M_S \\ M_S & L_{Sp} & M_S \\ M_S & M_S & L_{Sp} \end{bmatrix}, \quad [\mathbf{M}_{SR}]_{N_R \times 3} = \begin{bmatrix} \dots & -M_{SR} \cdot \cos(\theta + k.a) & \dots \\ \dots & -M_{SR} \cdot \cos(\theta + k.a - \frac{2\pi}{3}) & \dots \\ \dots & -M_{SR} \cdot \cos(\theta + k.a - \frac{4\pi}{3}) & \dots \end{bmatrix}$$

and

$$[\mathbf{L}_R] = \begin{bmatrix} L_{Rp} + 2L_b + 2\frac{L_c}{N_R} & M_{RR} - L_b & M_{RR} & M_{RR} & \dots & M_{RR} - L_b \\ M_{RR} - L_b & L_{Rp} + 2L_b + 2\frac{L_c}{N_R} & M_{RR} - L_b & M_{RR} & M_{RR} & \dots \\ M_{RR} & M_{RR} - L_b & L_{Rp} + 2L_b + 2\frac{L_c}{N_R} & M_{RR} - L_b & M_{RR} & \dots \\ M_{RR} & \vdots & \vdots & \vdots & \vdots & \vdots \\ \vdots & \vdots & \vdots & \vdots & \vdots & \vdots \\ M_{RR} - L_b & M_{RR} & M_{RR} & \dots & M_{RR} - L_b & L_{Rp} + 2L_b + 2\frac{L_c}{N_R} \end{bmatrix}$$

Using the Park's matrix transformation in the stator, the equation (12) can be written as:

$$[\mathbf{V}_T] = [\mathbf{R}_G] [\mathbf{I}_T] + \frac{d}{dt} ([\mathbf{L}_G] [\mathbf{I}_T]) \quad (15)$$

where:

$$[\mathbf{V}_T] = [V_{0S} \ V_{dS} \ V_{qS} \ 0 \ 0 \ \dots \ 0 \ \dots \ 0]_{1 \times N_R + 4}^T$$

$$[\mathbf{I}_T] = [I_{0S} \ I_{dS} \ I_{qS} \ I_{R1} \ I_{R2} \ \dots \ I_{Rk} \ \dots \ I_e]_{1 \times N_R + 4}^T$$

and:

$$\begin{bmatrix} R_S & 0 & 0 & \vdots & 0 & 0 & \dots & \dots & 0 & \vdots & 0 \\ 0 & R_S & 0 & \vdots & 0 & -T_1 \sin(a) & \dots & \dots & -T_1 \sin(N_R - 1)a & \vdots & 0 \\ 0 & 0 & R_S & \vdots & T_1 & T_1 \cos(a) & \dots & \dots & T_1 \cos(N_R - 1)a & \vdots & 0 \\ \dots & \dots & \dots & \vdots & \dots & \dots & \dots & \dots & \dots & \vdots & \dots \\ 0 & 0 & T_1 & \vdots & R_{b0} + R_{b(N_R - 1)} + 2\frac{R_e}{N_R} & -R_{b0} & 0 & \dots & -R_{b(N_R - 1)} & \vdots & -\frac{R_e}{N_R} \\ 0 & -T_1 \sin(a) & T_1 \cos(a) & \vdots & \ddots & \ddots & \ddots & \ddots & \ddots & \vdots & \ddots \\ \vdots & \vdots & \vdots & \vdots & 0 & -R_{b(k-1)} & R_{b_k} + R_{b(k-1)} + 2\frac{R_e}{N_R} & -R_{b_k} & 0 & \vdots & \vdots \\ \vdots & \vdots \\ 0 & -T_1 \sin(N_R - 1)a & T_1 \cos(N_R - 1)a & \vdots & -R_{b(N_R - 1)} & 0 & \dots & -R_{b(N_R - 2)} & R_{b(N_R - 1)} + R_{b(N_R - 2)} + 2\frac{R_e}{N_R} & \vdots & -\frac{R_e}{N_R} \\ \dots & \dots & \dots & \vdots & \dots & \dots & \dots & \dots & \dots & \vdots & \dots \\ 0 & 0 & 0 & \vdots & -\frac{R_e}{N_R} & \dots & \dots & \dots & -\frac{R_e}{N_R} & \vdots & R_e \end{bmatrix}$$

with:

$$T_1 = \sqrt{\frac{3}{2}} \omega_R M_{SR}$$

and

$$\begin{bmatrix} L_S + 2M_S & 0 & 0 & \vdots & 0 & 0 & \dots & \dots & 0 & \vdots & 0 \\ 0 & L_S - M_S & 0 & \vdots & \sqrt{\frac{3}{2}} L_{SR} & \sqrt{\frac{3}{2}} L_{SR} \cos(a) & \dots & \dots & \sqrt{\frac{3}{2}} L_{SR} \cos(N_R - 1)a & \vdots & 0 \\ 0 & 0 & L_S - M_S & \vdots & 0 & \sqrt{\frac{3}{2}} L_{SR} \sin(a) & \dots & \dots & \sqrt{\frac{3}{2}} L_{SR} \sin(N_R - 1)a & \vdots & 0 \\ \dots & \dots & \dots & \vdots & \dots & \dots & \dots & \dots & \dots & \vdots & \dots \\ 0 & \sqrt{\frac{3}{2}} L_{SR} & 0 & \vdots & L_{Rp} + 2L_b + 2\frac{L_e}{N_R} & M_{RR} - L_b & M_{RR} & \dots & M_{RR} - L_b & \vdots & -\frac{L_e}{N_R} \\ 0 & \sqrt{\frac{3}{2}} L_{SR} \cos(a) & \sqrt{\frac{3}{2}} L_{SR} \sin(a) & \vdots & \ddots & \ddots & \ddots & \ddots & \ddots & \vdots & \ddots \\ \vdots & \vdots & \vdots & \vdots & M_{RR} & M_{RR} - L_b & L_{Rp} + 2L_b + 2\frac{L_e}{N_R} & M_{RR} - L_b & M_{RR} & \vdots & \vdots \\ \vdots & \vdots \\ 0 & \sqrt{\frac{3}{2}} L_{SR} \cos(N_R - 1)a & \sqrt{\frac{3}{2}} L_{SR} \sin(N_R - 1)a & \vdots & M_{RR} - L_b & M_{RR} & \dots & M_{RR} - L_b & L_{Rp} + 2L_b + 2\frac{L_e}{N_R} & \vdots & -\frac{L_e}{N_R} \\ \dots & \dots & \dots & \vdots & \dots & \dots & \dots & \dots & \dots & \vdots & \dots \\ 0 & 0 & 0 & \vdots & \frac{L_e}{N_R} & \dots & \dots & \dots & \frac{L_e}{N_R} & \vdots & L_e \end{bmatrix}$$

The mechanical equation is:

$$\frac{d}{dt} \omega_m = \frac{1}{J_m} (C_e - C_r) \quad (16)$$

where:

$$\omega_m = \frac{d\theta_m}{dt}$$

and

$$C_e = \sqrt{\frac{3}{2}} p M_{SR} \left\{ I_{qS} \sum_{k=0}^{N_r-1} I_{k+1} \cos(ka) - I_{dS} \sum_{k=0}^{N_r-1} I_{k+1} \sin(ka) \right\}$$

4. Incipient rotor faults simulation

For a three-phase squirrel cage motor with N_R -bars and one end ring current, equations (15) and (16) can be resolved using the Runge-Kutta method.

Using a computer program written in Matlab, the partial or the total breakage fault in the bar is modeled by the linearly change of the value of the resistance R_{bF} named fault bar resistance. Thus we consider that the variation of the resistance R_{bF} as a function of time is given by the relation (17).

$$R_{bFk} = R_b \cdot (1 + \alpha(t - t_0)) \quad (17)$$

The first case assumes that a rotor bar is totally broken at $t=1s$. The second one illustrates the medium cases when the partial broken bar time evolution is obtained with $\alpha=14.5$. The third case characterizes the slowly broken bar situation with $\alpha=5.8$. The R_{bF} -time evolution is shown in Fig.4.

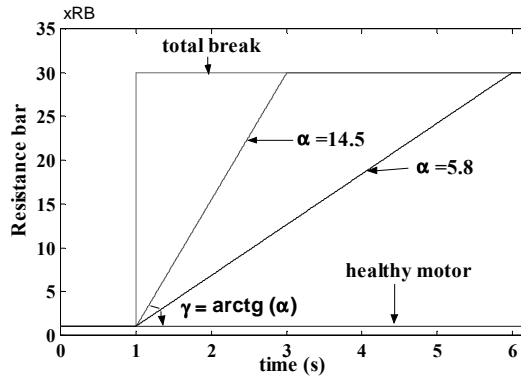


Fig. 4 Variation order of resistance broken bar $N^{\circ}2$

The fault is considered in the k^{th} bar and the fault matrix $[R_F]$ is added to the rotor sub-matrix:

$$[R_F] = \begin{bmatrix} 0 & \dots & 0 & \dots & \dots & 0 \\ \vdots & \dots & \vdots & \vdots & \dots & \vdots \\ \vdots & \dots & 0 & 0 & \dots & 0 \\ 0 & 0 & R_{bFk} & -R_{bFk} & 0 & 0 \\ 0 & 0 & -R_{bFk} & R_{bFk} & 0 & 0 \\ \vdots & \vdots & 0 & 0 & \vdots & \vdots \\ \vdots & \vdots & \vdots & \vdots & \vdots & \vdots \\ \vdots & \vdots & \vdots & \vdots & \vdots & \vdots \end{bmatrix} \quad (18)$$

5. Results and discussion

The curves of speed, electromagnetic torque, and stator and rotor currents versus time are plotted with applied constant load at 0.6 s. We consider that the failure of a bar starts at the moment $t = 1s$ as shown respectively on Fig. 5, 6, 7 and 8.

The oscillations shown on the curves of figures 5 and 6 justify the presence of rotor bar defect inside the machine.

The effect of the rotor bar resistance variation results in an increase in the amplitude of the vibrations (Fig. 5).

The current oscillations observed in the fissured bar follow a deadened pattern because the partial break tends towards a total break (Fig.8).

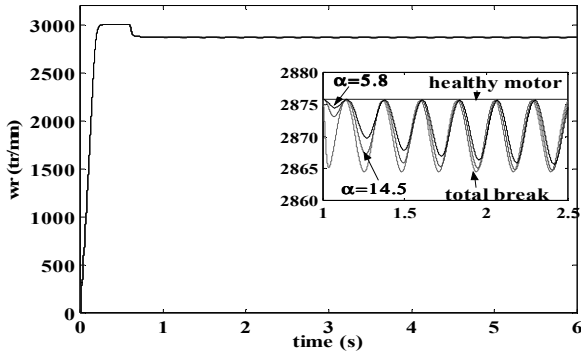


Fig. 5: Electrical speed for the healthy motor and broken rotor bar N°2

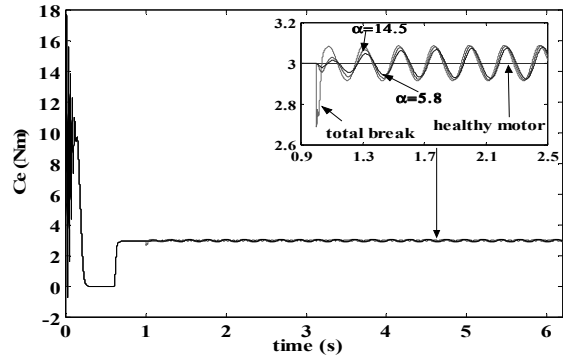


Fig. 6: Torque for healthy motor and broken bar N°2

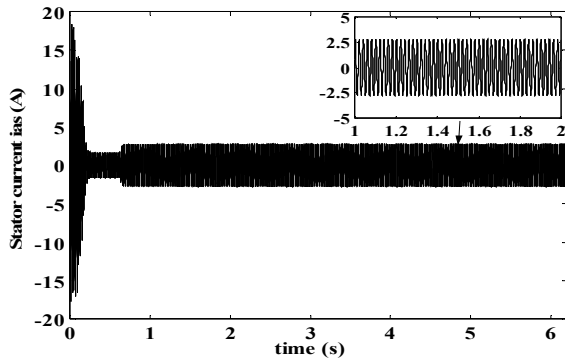


Fig. 7: Stator current of phase 1

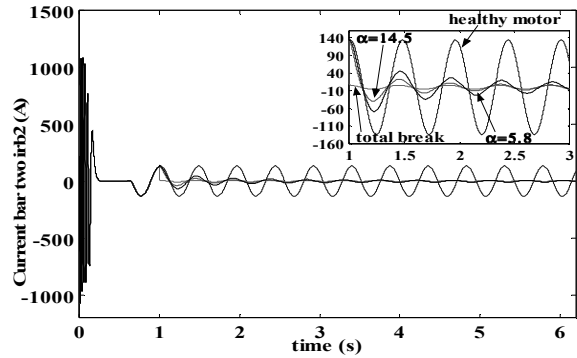


Fig. 8: Rotor bar current with broken bar N°2

The direct analysis of the stator current, as shown on Fig.7, does not make the presence of the defect obvious because of the weak modulation of the sinusoidal current in permanent state.

The appearance of lines at the frequencies $(1 \pm 2g)f_s$ on the stator current spectrum obtained in permanent state and presented in Fig. 9 is highlighted by using Fourier Fast Transform FFT.

Figure 8 presents respectively the real rotor bar current versus-time. We can observe the broken bar evolution for three above cases ($\alpha = 5.8, 14.5$ and ∞).

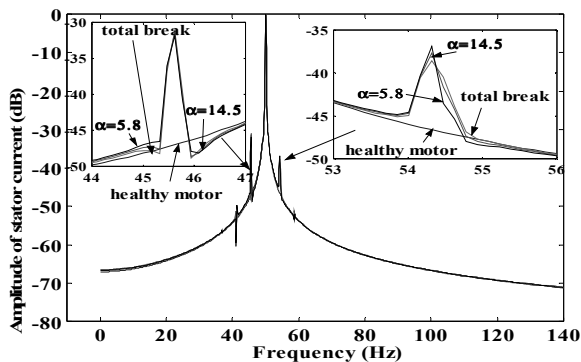


Fig. 9: FFT of the stator current for the healthy motor and one broken bar N°2

	$\alpha \rightarrow \infty$	$\alpha=14.5$	$\alpha = 5.8$
$f_1=(1-2g)f_s$ (Hz)	45.6300	45.6300	45.6400
f_1 (Hz)	45.6235	45.6238	45.6232
$f_2=(1+2g)f_s$ (Hz)	54.3700	54.3700	54.3600
f_2 (Hz)	54.3217	54.3211	54.3199
A_1 (dB)	-31.1050	-31.3084	-31.9652
A_2 (dB)	-38.5902	-37.7555	-37.0051

Tab.1: Current spectrum analysis

We can note that the failure in the rotor bar is detected whatever the type of broken bar time-evolution law. f_1 and f_2 are the lower and the upper frequencies deduced by using the maximum values of the curves (Fig. 9). The frequencies calculated according to the relation and deduced from the Fig. 9 show a good agreement to one another as indicated in the table 1. These results are very close to those obtained from the relation $(1 \pm 2g)f_s$, which was experimentally validated by different authors [16].

For a healthy motor, the curve of Lissajous i_d (i_q) is a circle. When the default occurs in the bar, this circle is slightly deformed and becomes an ellipse as shown on Fig. 11.

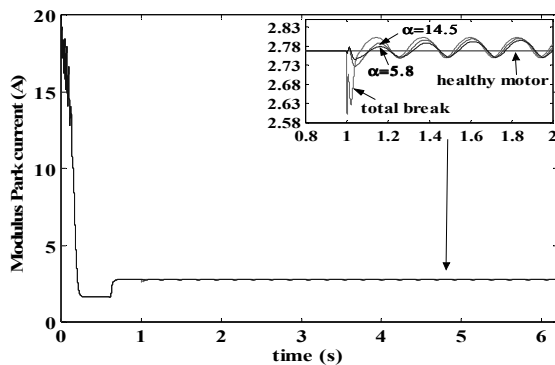


Fig. 10: Park current

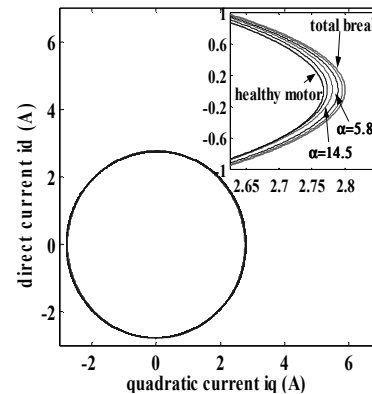


Fig. 11: Extended Park current

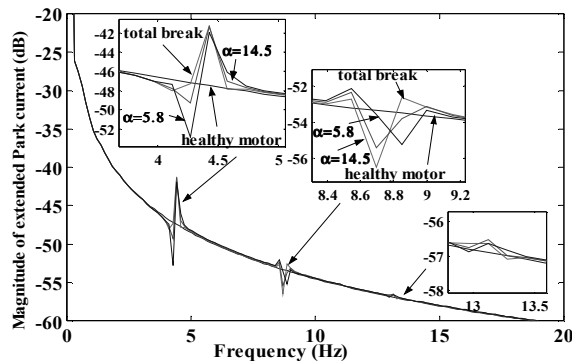


Fig. 12: Extended Park current spectrum analysis

	$\alpha \rightarrow \infty$	$\alpha=14.5$	$\alpha = 5.8$
$f_1=2.g.f_s$ (Hz)	4.3736	4.3656	4.3551
f_1' (Hz)	4.4248	4.4266	4.4248
$f_2=4.g.f_s$ (Hz)	8.7473	8.7313	8.7102
f_2' (Hz)	8.6962	8.6977	8.8512
$f_3=6.g.f_s$ (Hz)	13.1209	13.0969	13.0653
f_3' (Hz)	13.1186	13.1217	13.1217
A_1 (dB)	-41.3286	-41.4808	-42.0591
A_2 (dB)	-56.4675	-55.4509	-55.1968
A_3 (dB)	-56.6654	-56.5623	-56.6654

Tab.2: Park current spectrum analysis

In permanent state, the appearance of harmonics at the frequencies $(2.k.g).f_s$, $k=1, 2, 3...$ [18] on the spectrum of the extended Park current (Fig 10) is highlighted by using Fourier Fast Transform FFT as presented on Fig. 12.

The table 2 summarizes frequencies and amplitudes of current spectrum in the case of incipient rotor bar faults. The frequencies calculated according to the relation and deduced from the Fig.12 show a good agreement to one another as indicated in the table 2. The both above current spectrum analyses indicate the fault presence in rotor bar since its existence thanks to the appearance of lines at specific fault frequencies.

In the case of a rotor bar failure, the distribution of the RMS values bars currents also shows the nature of the failure (partial or total break), as shown on Fig. 13-a, b, c, d.

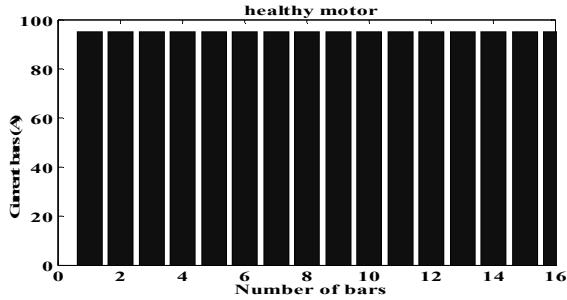


Fig. 13-a RMS values current bars of the healthy motor at $t=1.5$ s

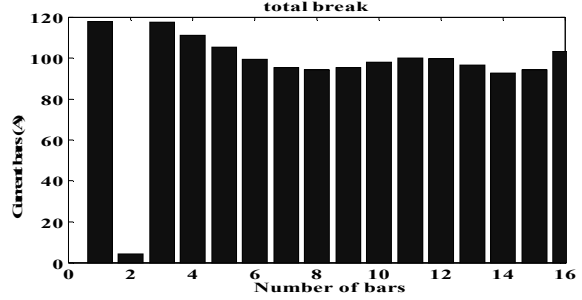


Fig. 13-b RMS values current bars with one broken bar at $t=1.5$ s ($\alpha \rightarrow \infty$)

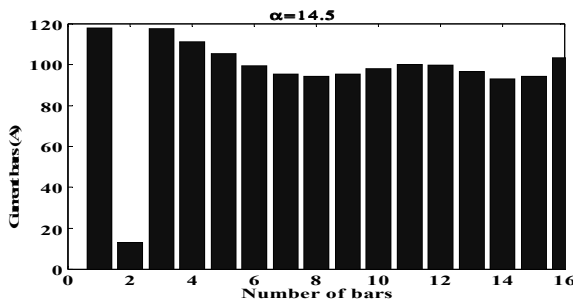


Fig. 13-c RMS values current bars with one partial bar break at $t=1.5$ s ($\alpha=14.5$)

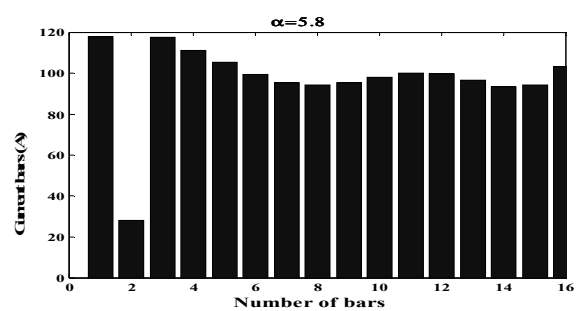


Fig. 13-d RMS values current bars with one partial bar break at $t=1.5$ s ($\alpha=5.8$)

5. Conclusion

This paper presents computer simulation of incipient rotor bar fault in induction motor for diagnosis purpose. Based on a mathematical model of the induction motor, the computer simulation takes into account the variation of the rotor resistance from a partial to a total break of one rotor bar.

Spectrums analysis of the stator current and *Park* vector current shows only the presence of a bar defect without specifying the nature of this defect (partial or total break). However, the magnitude of the default can be highlighted by the analysis of speed or torque responses.

Moreover, since current spectrums obtained in simulation in the presence of rotor bar fault are nearly the same as the ones obtained in experimental cases as described in [16], we can deduce that the evolution law suggested for incipient fault on the rotor bar models rather well the physical phenomenon.

Machine parameters

$P_0=1.1$ kW $N_s=160$ $N_R=16$ $R_s=7.58$ Ω $L_{sf}=26.5$ mH $2p=2$ $R_b=1.5$ $\mu\Omega$ $R_c=1.5$ $\mu\Omega$
 $L_c=0.1$ μ H $L_b=0.1$ μ H $D=71.5$ mm $l=65$ mm $J_m=0.0054$ Nms² $f_s=50$ Hz $V=220$ V

List of principal symbols

P_0 power of the machine

l, e	rotor length and air-gap length respectively
N_R, N_s	number of rotor bars and number of effective series connected coils per stator phase respectively
R_e	resistance of end ring segment between two adjacent rotor bars
R_a	resistance of stator phase a winding
R_b, R_c	rotor bar and rotor ring resistance respectively
D, B	air- gap mean diameter and magnetic flux density respectively
L_b	leakage inductance of rotor bar
L_e	leakage inductance of end ring segment between two adjacent rotor bars
μ_0	permeability of air gap space
r_g	mean radius of the air-gap
C_e	electromagnetic torque
J_m, g	inertia moment and slip respectively
ω_r, ω_m	electric and mechanical angular velocity
I_{S_n}	stator phases currents; $n=1, 2, 3$ (phase number)
α	resistance time ratio
f_s	stator supply frequency
f_1, f_2	lower and upper frequencies of current spectrum respectively
A_1	current amplitude at the lower frequency of current spectrum
A_2	current amplitude at the upper frequency of current spectrum
t_0	moment of the incipient failure
mmf	magneto motrice force

References

1. Yuen Chow, MO, "Guest Editorial Special Section on Motor Fault Detection and Diagnosis". *IEEE Transactions on Industrial Electronics*, Vol 47, N° 5, October 2000, pp 982-983.
2. W.T. Thomson, D. Rankin, "Case histories of on-line rotor cage fault diagnosis, condition monitoring" *Conferences proceeding, Swansea.*, 1987, pp 789-819.
3. Chow, T.W.S, Fel G, "Three phase induction machine asymmetrical faults identification using bi-spectrum", *IEEE Transactions on Energy Conversion.*, 10(4), December 1992, pp 88-93.
4. A.G. Innes, R. Langman, "The detection of broken bars in variable speed induction motor drives", *International Conferences on Electrical Machines*, 1994.
5. Randy R. Schoen, T.G. Habetler, Effects of time-varying loads on rotor fault detection in induction machines", *IEEE Transactions on industry Applications*, 31(4), July-August 1995, pp 900-906.
6. R.F. Walliser, C.F. Landy, "Determination of inter bar currents in the detection of broken bars in squirrel cage induction motors", *IEEE Transaction on Energy Conversion*, 9(1), March 1994, pp 152-158.

7. J.R. Cameron, W.T. Thomson, A.B. Dow, "One Line current monitoring of induction motors a method for calculating the level of air gap eccentricity", *IEE Conferences on Electrical Machines and Drives*, 1987, pp 173-177.
8. J. Penman, H.G. Sedding, B.A. Lloyd, W.T. Fink, "Detection and location of inter turn short circuits in the stator winding of operating motors", *IEEE Transaction on Energy Conversion*, February 1994, pp 463-474.
9. T.G. Phemister, G. Gregorgy, "Monitoring fractional shorted turns on generator rotors", *International Conference on Electrical Machines*, 1992.
10. J. Ederman, R.J Kerkman, D. Schlegel, G. Skibinski, "Effect of PWM inverters on AC motor bearing currents and shaft voltages", *APEC '95*, 1995, pp 24-28.
11. Randy R. Schoen., Habetler, T.G , Kamran, F , Batheld, R.G, "Motor bearing damage detection using stator currents monitoring", *IEEE Transaction on industry Applications*, 31(6), November-December 1995, pp 1274-1279.
12. Lipo ,A. R.T.A , "Complex vector Model of the Squirrel-Cage Induction Machine Including Instantaneous Rotor bar Currents", *IEEE Transaction on Industry Application*, Vol.35, N°6, Nov/Dec, 1999 pp 1333-1340.
13. Novotny, D. W ,Lipo, T.A , "Victor control and dynamics of AC drives", *Clarendon Press Oxford* 1996
14. M. Eltabach, A. Charara and I. Zein, "A Comparison of External and Internal Methods of Signal Spectral Analysis for Broken Rotor Bars Detection in Induction Motors", *IEEE Transactions On Industrial Electronics*, Vol. 51, N° 1, February 2004, pp 107-121
15. S. M. A. Cruz and A. J. M. Cardoso, "Rotor cage fault diagnosis in three-phase induction motors by extended Park's vector approach," *Elect. Mach. Power Syst.*, vol. 28, 2000, pp 289-299.
16. G. Didier, H. Razik and A. Rezzoug, "On the Experiment Detection of Incipient Rotor Fault of an Induction Motor", *IEEE*, pp 913-916, 2003.
17. A. Menacer, M.S. Nait Said, A.H. Benakcha, S. Drid, "Stator Current Analysis of Incipient Fault Into Asynchronous Motor Rotor Bars Using Fourier Fast Transform", *Journal of Electrical Engineering*, Vol. 5-6, 2004, pp 122-130, Slovakia.
18. Mark. Fenger, Blake A. Lloyd and William T. Thomson, "Development of a tool to detect faults in induction motors via current signature analysis", *IEEE*, 2003, pp 37-46
19. S. Moreau, J.C. Trigeassou, G. Champenois, J.P. Gaubert, "Diagnosis of Induction Machines : a procedure for electrical fault detection and localization", *IEEE, SDEMPED '99*, Gijon, 1-3 septembre 1999, pp. 225-230.